Automatic Identification of Critical Landmarks on the Third Ventricle

Peter Čech Philippe C. Cattin Gábor Székely

Computer Vision Laboratory, ETH Zurich, 8092 Zurich, Switzerland
{cech,cattin,szekely}@vision.ee.ethz.ch

Abstract: As of today, multiple diseases have been associated with shape and volumetric changes in the brain's ventricular system. Undoubtedly, the transport mechanisms in the cerebrospinal fluid play an important role, but the knowledge about the related phenomena is still limited.

Computational fluid dynamics calculations, which may shed light on the underlying mechanisms, need detailed, topologically correct models of the ventricles in order to perform realistic flow simulations. In preliminary experiments some anatomical structures have been identified, which have major influence on the flow characteristics. In this paper we propose an automatic method for extraction of those landmarks, which will also be useful in a later stage to initialize and to guide the segmentation process of the third ventricle.

1 Introduction

As of today multiple diseases can be associated with shape and volume changes in the ventricular system of the brain and there is intensive clinical research focusing on the topic. Undoubtedly, flow and associated transport phenomena of the cerebrospinal fluid (CSF) play an important role, but the knowledge about the subject is still rather limited. Computational fluid dynamic (CFD) simulations of the CSF performed on realistic models promise to broaden this knowledge and might even become a valuable diagnostic tool.

Although tedious manual segmentation is still common in clinical applications, a shift towards semi- and fully automatic segmentation techniques for the third ventricle would be desirable. To overcome the complications such as thin separation membranes between the ventricular and external CSF, an automatic segmentation algorithm for the third ventricle has to incorporate prior anatomical knowledge. Wu et al. [WPW+03] used an expectation maximization driven deformation of an anatomical atlas, whereas Schnack et al. [SPB+01] and Xia et al. [XHA+03] used region growing combined with anatomical knowledge to correctly identify components of the ventricular system that otherwise would appear disconnected in the image. All of the above methods can split the ventricular system into disconnected compartments when the connection between them is not apparent in the data. Furthermore, Schnack and Xia are using simple planar boundaries to prevent the segmentation of the third ventricle from leaking into extraventricular CSF. The resulting inaccuracies in the shape of the third ventricle would alter the outcome of the CFD sim-

ulation as it requires both correct topology and realistic geometry. Preoperative planning can also benefit from improved segmentation algorithms.

A variety of landmark extraction techniques for 3D volumes have been presented in the literature. Gu and Tjahjadi [GT02] employ bandpass filters to detect salient features in the images, whereas De Vries and Verbeek [dVV00] are using eigenanalysis of the gradient structure tensor to detect and classify them. An extensive evaluation of derivative based point landmark extraction methods was performed by Rohr and Hartkens [Roh97, HRS02]. The work of Worz and Rohr [WR05] offers not only the landmark localization, but the fitting of parametric intensity models also offers a shape description of the landmarked structure. The prominent position of the anterior and posterior commissure as stereotaxic landmarks led to specialized extraction algorithms (e. g. [PHA$^+$06]), but almost exclusively on T1 imagery.

2 Method

The third ventricle has a complex anatomy as can be seen in Figure 1. It includes multiple recesses, neural fiber tracts connecting the cerebral hemispheres and a body of choroid plexus tissue. The size of the recesses varies, occasionally they are reduced to mere bumps. The anterior wall (between the AC and the tip of the OR) has only a thin separation membrane to a body of extraventricular CSF in the anterior direction. Preliminary CFD simulations showed that the anterior wall and the recesses are important factors for the flow.

The proposed approach can be summarized as follows. The selected interest points are identified in a hierarchical fashion, starting with the entry point of the cerebral aqueduct and followed by the AC and PC which can be detected most robustly. We search for the other landmarks sequentially, while spatial information form previously extracted interest points is used to limit the search regions of the still unknown ones. For each interest point, a set of candidates is extracted. Using anatomical knowledge, the interest point corresponding to a specific anatomical structure is selected from these candidates.

Our method relies on T2 weighted MRI images acquired on 3T Philips Intera Achieva scanner. Nine healthy volunteer data sets are divided into two groups. Group A contains three volumes[1] with an in-plane resolution of once 0.5 and twice 0.225 mm (interpolated by zero filling in the Fourier domain) and an inter-slice distance of 0.47 mm and 0.4 mm respectively. For Group B, the scanning sequence was modified[2] to reduce imaging artifacts. The Group B contains six volumes with an in-plane resolution of 0.45 mm and an inter-slice distance of 0.6 mm.

Many important anatomical structures have tips or are of tubular shape. They can therefore be detected as point or line features. In case of the third ventricle we use different methods for (1) tip landmarks and (2) landmarks for short tubular structures.

[1] SE, TE/TR 130/2800, 160/2000 and 160/2325 respectively, flip angle $90°$

[2] SE, TE/TR 150/2000, flip angle $90°$

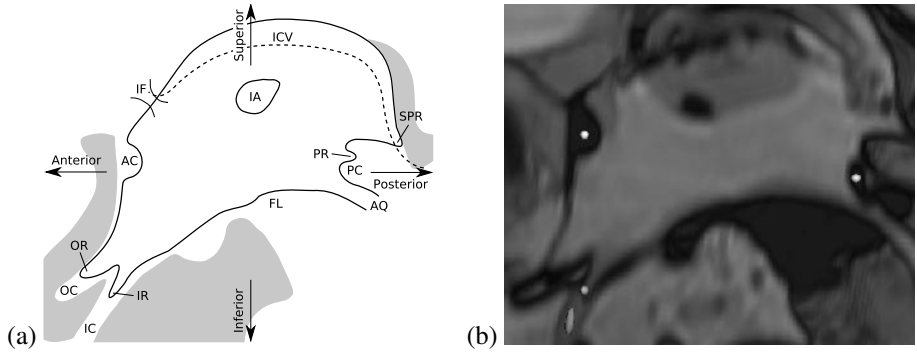

Figure 1: (a) Anatomy of third ventricle. Extraventricular CSF is marked in light gray. **AC** Anterior commissure, **AQ** Cerebral aqueduct, **FL** Floor of the third ventricle, **IA** Interthalamic adhesion, **IC** Infundibular chiasm, **ICV** Internal cerebral veins, **IF** Interventricular foramen, **IR** Infundibular recess, **OC** Optic chiasm, **OR** Optic recess, **PC** Posterior commissure, **PR** Pineal recess, **SPR** Suprapineal recess (b) Selected landmarks overlaid on a MRI dataset.

Tip landmarks: Extraction of tip-like structures is based on the gradient structure tensor $GST_{\sigma,\psi}$ presented in [dVV00, HRS02]. Through an extensive evaluation Hartkens et al. [HRS02] found, that the determinant of the gradient structure tensor offered consistently good performance under a wide range of conditions.

Tubular landmarks: To detect the tubular landmarks, first the eigenvalues and eigenvectors of the Hessian matrix are extracted for each voxel. Based on the eigenvalues, a vesselness measure $V(X)$ is derived using the method proposed in [SNA+97]. The vesselness measure represents a likelihood of a voxel to be in the center of a tubular structure.

Other tubular structures, mainly vessels, can be present in the region of interest (ROI) for the landmark, but their orientation differs from the orientation $\vec{d}$ of the landmark structure. Therefore, we suppress the vesselness measure in the structures strongly deviating from $\vec{d}$, while maintaining it in the well aligned structures. The attenuated vesselness measure $V'(X)$ is computed as $V'(X) = V(X)|\vec{d} \cdot \vec{e}|/(I_X+b)$, where $\vec{e}$ is the direction along the local structure[3] at X, I_X is the intensity of the voxel X and b is an intensity bias to avoid division by zero and at the same time to suppress the influence of the noise in the image. As a result, the voxels belonging to bright structures and the voxels of structures with unfavorable orientation end up with a lower measure than the voxels in favorably oriented dark structures. We set the value of b to 1% of the estimated CSF threshold.

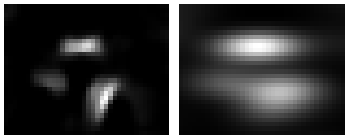

Figure 2: Attenuated vesselness (left) and its anisotropic integration in the preferred left-right direction (right). Upper blob is the AC.

Next, we integrate the attenuated vesselness image $V'(X)$ with an anisotropic Gaussian kernel (of width σ_{LR}, σ_{IS}, and σ_{AP})[4] with a large standard deviation in the expected

[3] an eigenvector corresponding to the eigenvalue with smallest absolute value

[4] coordinates are corresponding to the left-right (LR), anterior-posterior (AP) and inferior-superior (IS) axis

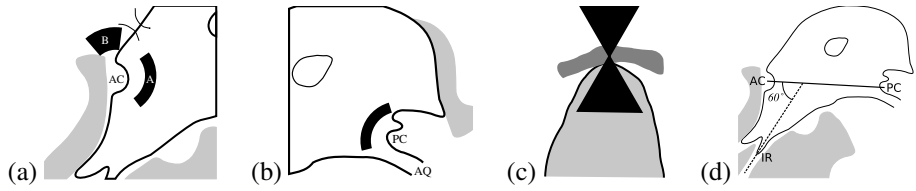

Figure 3: Details of intensity regions for the AC (a) and the PC (b); sagittal view. (c) Expected orientation of both AC and PC is left-right, structures deviating more than 60° (black area) are rejected in the prefiltering step; axial view. (d) Expected orientation of the infundibular recess and chiasm; sagittal view.

direction and a small in the perpendicular directions (Figure 2). This smoothing not only causes isolated high response voxels to be suppressed, but also further attenuates clusters deviating from the expected orientation. The local maxima of the integrated image are then selected as candidates of the structure. The representative of the structure is selected from the candidates according to rules derived from local anatomy.

Localization of Entry Point of Cerebral Aqueduct: The first step is the detection of the entry point of the cerebral aqueduct. There are multiple ways to obtain it, but as our investigation of the third ventricle is performed in the context of the segmentation of the whole ventricular system, we detect it by following the aqueduct from the fourth ventricle.

Localization of the Posterior Commissure: The PC appears as a dark tubular structure in the posterior part of the third ventricle just superior to the entry point of the cerebral aqueduct. It is oriented along the left-right axis. To restrict the search area, a ROI of size $5\ \mathrm{mm} \times 10\ \mathrm{mm} \times 10\ \mathrm{mm}$ is placed $2\ \mathrm{mm}$ anteriorly and $2\ \mathrm{mm}$ inferiorly from the entry point of the aqueduct. Using the detector for short tubular structures with a preferred left-right orientation $\vec{d}$ and the Gaussian filter kernels $\sigma_{LR} = 2.5\ \mathrm{mm}$, $\sigma_{IS} = \sigma_{AP} = 0.75\ \mathrm{mm}$, the set of candidates is extracted. All candidates located in a CSF region are rejected. Additionally, we reject the candidates with a direction deviating more than 60° from the left-right axis (Figure 3(c)). The region superior to the PR contains structures locally similar to the PC and usually produces a false candidate. Erroneous identification can be avoided by selecting the candidate located just above the cerebral aqueduct. To improve LR localization, we project the landmark to the symmetry plane of the third ventricle.

Localization of Anterior Commissure: Similar to the PC, the AC appears as a dark tubular structure in the anterior part of the third ventricle. To limit the search area, we use a ROI of size $12\ \mathrm{mm} \times 16\ \mathrm{mm} \times 22\ \mathrm{mm}$ with its center placed $23\ \mathrm{mm}$ anteriorly to the PC. The dimensions of the ROI was designed to account for the uncertainties in the size and orientation of the third ventricle. The extraction of the AC candidates follows the approach used for the PC. The further filtering rules are derived from the local anatomy surrounding the AC and are depicted in Figure 3(a). The average intensity of the region A must be below the CSF threshold, whereas the average intensity of the region B must be above the threshold. The resulting AC candidates are then rated according to the value

ordering

Group	AC	PC	IR	OR
A	1.02 (0.52)	1.15 (0.60)	0.51 (–) [2]	2.27 (0.11) [1]
B	0.73 (0.37)	0.86 (0.34)	1.06 (0.44) [1]	1.45 (0.72) [1]

Table 1: Average localization error and its standard deviation (both in mm) for the landmarks. The number of cases where the landmark detection failed is given in square brackets (these cases were excluded from the statistics).

of integrated vesselness in the left-right direction and the contrast ratio between regions A and B. The candidate with the highest product of the two measures is selected as the AC landmark.

Localization of Infundibular Recess: The landmark is located at the tip of the infundibular recess. It is localized in two phases. First, landmark candidates for the IC are searched for using the short tubular structure detector in a ROI of size $10\ \mathrm{mm} \times 14\ \mathrm{mm} \times 12\ \mathrm{mm}$, centered $17\ \mathrm{mm}$ inferior and $2\ \mathrm{mm}$ posterior to the AC. The expected orientation is at $60°$ inferior to the PC–AC, (see Figure 3(d)) while using an isotropic Gaussian filter kernel ($\sigma_{LR} = \sigma_{IS} = \sigma_{AP} = 1.25\ \mathrm{mm}$). In a first filtering stage, all candidates with a deviation larger than $45°$ from the expected orientation are discarded. Additionally, all candidates that are not surrounded by CSF in the plane perpendicular to the structure orientation are removed, too. The remaining candidates are passed to the second phase, where their corresponding tip is extracted using the determinant of the gradient structure tensor as described in the tip landmark detector. Lets recall the anatomy of the immediate surrounding of the infundibular recess, which extends inside the tube of the IC. The vesselness measure is not suitable for the detection of such double tube structures. Therefore, the chiasm candidate is always detected farther away from the third ventricle body. When we look at the cross-section perpendicular to the longitudinal axis of the tip or chiasm, we see a high intensity blob of the IR tip, surrounded by a ring of dark tissue of the chiasm, which is in turn surrounded by bright CSF area. We adjusted the iris filter [KM96] to rank the landmarks after filtering out the IR candidates that are not surrounded by the structure described above.

Optic Recess and the Anterior Wall: The OR is located in the lower end of the anterior wall. A body of extraventricular CSF is located anteriorly to it, separated only by a thin wall. Due to partial volume effects, often only a small part of this separation membrane is visible. The visible part of the separation wall is extracted and extrapolated as needed to cover the whole front of the optic recess. The segmentation starts from the AC and follows the low intensity sheet along the anterior wall. The tracing of the sheet is stopped when the ratio of the smallest and the largest eigenvalue of the Hessian matrix is above 0.5 (wall untraceable) or after $8\ \mathrm{mm}$ (whole wall extracted).

3 Results

The method was implemented in C++ using ITK [ITK]. Runtime performance was measured on a PC with $3.0\ \mathrm{GHz}$ Pentium 4 processor and 1GB of RAM. The extraction of the

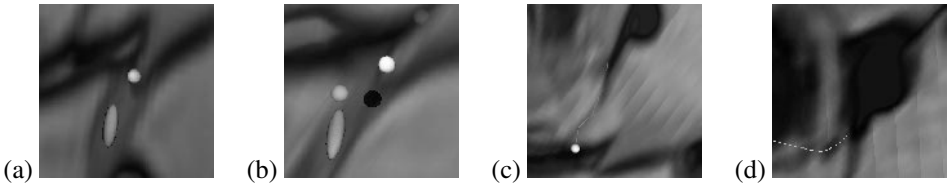

Figure 4: Results. (a) Example of successful extraction of an IR landmark (white dot), the ellipse denotes the IC landmark. (b) Wrongly detected IR landmark (black dot), the correct position is marked by a white dot, with more landmark candidates in the background. (c) Successful extraction of the anterior wall and the optic recess. (d) Our algorithm failed to locate the start of the anterior wall.

landmarks took $19 - 31$ s on lower resolution data sets and $138 - 200$ s on higher resolution data sets. The relatively high variation is due to the varying number of candidate points for the landmarks.

The method was tested on the nine datasets described earlier and compared with results from manual segmentation. The statistics of the deviations is given by Tab. 1. Figure 1(b) shows an example, where AC, PC and IR have been successfully detected.

The AC and PC have been correctly identified on all images of the test dataset. The detected position deviated from the manually extracted landmarks mostly in the lateral direction. Projected to the midsagittal plane, the two positions were at most one voxel apart.

The IR landmark was successfully identified in six cases. The landmarks were typically placed off-center as shown in Figure 4(a), whereas a typical manually placed landmark is located on the centerline of the recess. In group B for one case a landmark on the wall of the OC was ranked highest with the correct candidate being second (Figure 4(b)). In both erroneous cases in group A, no raw landmark was placed on the tip of the recess. These datasets show lower contrast in the region of the IR and the potential candidates were filtered out during the Gaussian smoothing step.

It has to be noted that a failure to locate a recess landmark does not necessarily imply an overall failure of the identification process, as a recess with a fixed geometry can be assumed in such cases. Although inaccurate, the resulting model will still be anatomically correct.

The anterior wall was successfully extracted from seven datasets (Figure 4(c)). The misidentification of the anterior wall occurred once in each group. For the case in group A our algorithm was unable to identify the beginning of the wall and for the one in group B the tracking was attracted by a ridge belonging to the extraventricular CSF (Figure 4(d)). In both cases the detection of the OR failed. Automatically extracted OR landmarks are being placed more inside the recess than the manually extracted ones.

4 Conclusions and Future Work

We presented a fully automated method for the extraction of landmarks in the third ventricle. The method incorporates a priori knowledge about the anatomy and the appearance of the structures and their immediate surrounding. Preliminary experiments on 9 datasets demonstrated that this localization can be performed robustly and with high accuracy.

The presented landmark extraction method can also be used to improve segmentation of the third ventricle for the purpose of preoperative planning.

While the results already allow the generation of patient-specific boundary conditions for the computational simulation of cerebral fluid flow in critical regions, our future goal is to develop a complete, automatic segmentation system for the third ventricle, using the identified landmarks for the initialization of a deformable model and for the guidance of its evolution. Additionally, we are currently developing classification methods allowing to accurately locate the choroid plexus within the third ventricle.

References

[dVV00] G. de Vries and P.W. Verbeek. Scale-adaptive landmark detection, classification and size estimation in 3D object-background images. In *Proc. of ICPR 2000*, volume 3, pages 1014–1017, Barcelona, Spain, September 2000.

[GT02] I. Y-H. Gu and T. Tjahjadi. Multiresolution Feature Detection Using a Family of Isotropic Bandpass Filters. In *IEEE Transactions on Systems, Man, and Cybernetics, Part B: Cybernetics*, volume 32, pages 443–454, August 2002.

[HRS02] T. Hartkens, K. Rohr, and H. S. Stiehl. Evaluation of 3D Operators for the Detection of Anatomical Point Landmarks in MR and CT Images. *Computer Vision and Image Understanding*, 86(2):118–136, 2002.

[ITK] The Insight Segmentation and Registration Toolkit. http://www.itk.org.

[KM96] H. Kobatake and M. Murakami. Adaptive Filter to Detect Rounded Convex Regions: Iris Filter. In *Proc. of ICPR'96*, volume 2, pages 340–344, Vienna, August 1996.

[PHA+06] K.N. B. Prakash, Q. Hu, A. Aziz, et al. Rapid and automatic localization of the anterior and posterior commissure point landmarks in MR volumetric neuroimages. *Academic Radiology*, 13(1):36–54, January 2006.

[Roh97] Karl Rohr. On 3D differential operators for detecting point landmarks. *Image and Vision Computing*, 15(1):219–233, January 1997.

[SNA+97] Y. Sato, S. Nakajima, H. Atsumi, et al. 3D multi-scale line filter for segmentation and visualization of curvilinear structures in medical images. SPL Technical Report #44, SPL Brigham and Women's Hospital, Boston, Massachusetts, USA, April 1997.

[SPB+01] H. G. Schnack, H. E. Hulshoff Pol, W. F. C. Baaré, et al. Automatic Segmentation of the Ventricular System from MR Images of the Human Brain. *NeuroImage*, 14:95–104, July 2001.

[WPW+03] Y. Wu, K. M. Pohl, S. K. Warfield, et al. Automated Segmentation of Cerebral Ventricular Compartments. In *Proc. of ISMRM'2003*, Toronto, Ontario, Canada, July 2003.

[WR05] S. Wörz and K. Rohr. Localization of Anatomical Point Landmarks in 3D Medical Images by Fitting 3D Parametric Intensity Models. *Medical Image Analysis*, 2005.

[XHA+03] Y. Xia, QM. Hu, A. Aziz, et al. Knowledge-Driven Automated Extraction of the Human Cerebral Ventricular System from MR Images. In *Proceedings of IPMI 2003*, July 2003.